

# Chemical Science

Accepted Manuscript

This article can be cited before page numbers have been issued, to do this please use: S. Groni, S. Akbaba, U. Otgonbayar, J. Forté, S. M. Huber, S. Kasemthaveechok, B. Schöllhorn and C. Fave, *Chem. Sci.*, 2026, DOI: 10.1039/D6SC02883G.



This is an Accepted Manuscript, which has been through the Royal Society of Chemistry peer review process and has been accepted for publication.

Accepted Manuscripts are published online shortly after acceptance, before technical editing, formatting and proof reading. Using this free service, authors can make their results available to the community, in citable form, before we publish the edited article. We will replace this Accepted Manuscript with the edited and formatted Advance Article as soon as it is available.

You can find more information about Accepted Manuscripts in the [Information for Authors](#).

Please note that technical editing may introduce minor changes to the text and/or graphics, which may alter content. The journal's standard [Terms & Conditions](#) and the [Ethical guidelines](#) still apply. In no event shall the Royal Society of Chemistry be held responsible for any errors or omissions in this Accepted Manuscript or any consequences arising from the use of any information it contains.

## ARTICLE

## Redox Activation of Halogen-Bonding Catalysts for Organic Synthesis

Sihem Groni,<sup>a†</sup> Sercan Akbaba,<sup>b†</sup> Uchral Otgonbayar,<sup>a</sup> Jérémy Forté,<sup>a</sup> Stefan M. Huber,<sup>c</sup> Sitthichok Kasemthavechok,<sup>\*a</sup> Bernd Schöllhorn<sup>\*d</sup> and Claire Fave<sup>\*a</sup>Received 00th January 20xx,  
Accepted 00th January 20xx

DOI: 10.1039/x0xx00000x

Among non-covalent interactions, halogen bonding (XB) has emerged as a sophisticated tool for molecular assembly and catalysis, distinguished from its hydrogen bonding (HB) analogues by its superior directionality and the high polarizability of the halogen atom. These characteristics offer unique opportunities for fine-tuning the strength and the geometry of this interaction to achieve targeted functionalities. Furthermore, the use of a redox-active moiety enables a controlled increase of the XB donor strength upon oxidation, effectively activating the XB donor catalyst. Herein, we report the rational design and the synthesis of ferrocene-based XB donors. Characterization of the fundamental XB interactions in the system was performed through a synergistic approach involving single-crystal X-ray diffraction and solution-phase binding studies. Density Functional Theory (DFT) analysis reveals a significant amplification of the 'σ-hole' intensity upon oxidation, a feature we exploit to drive catalytic turnover. Notably, these redox-switchable iodoferrocene derivatives serve as potent catalysts for XB-mediated Friedel–Crafts alkylation reactions, even in competitive polar solvents—a challenging environment for traditional XB catalysis. This work demonstrates the efficacy of charge modulation by redox activation in fine-tuning XB strength for organic transformation.

## Introduction

Organocatalysis has transformed synthesis by facilitating molecular transformation under mild and metal-free conditions.<sup>1–4</sup> Enhancing catalytic activity in solution through the combination of external stimuli and supramolecular chemistry remains an exciting challenge.<sup>5–7</sup> Among supramolecular interactions, halogen bonding (XB) has attracted considerable interest across chemistry and biochemistry owing to its distinctive features, particularly its pronounced directionality. Beyond its well-established conceptual foundations in crystal engineering, molecular recognition, and biomolecular interactions, XB has recently emerged as a powerful tool in organic synthesis even if it remains a weak interaction.<sup>8–12</sup> This renewed attention stems from the presence of a partially electron-deficient region—known as the "σ-hole"—on halogen atoms.<sup>13</sup> Acting as a Lewis acid, the σ-hole enables XB donors to engage in specific attractive interactions with Lewis bases. In the context of organic synthesis, the Lewis bases involved are typically weaker than those employed in other applications of halogen bonding.<sup>14,15</sup> Consequently, strategies to enhance halogen-bond

strength are crucial for expanding its utility and effectiveness in promoting organic reactivity.

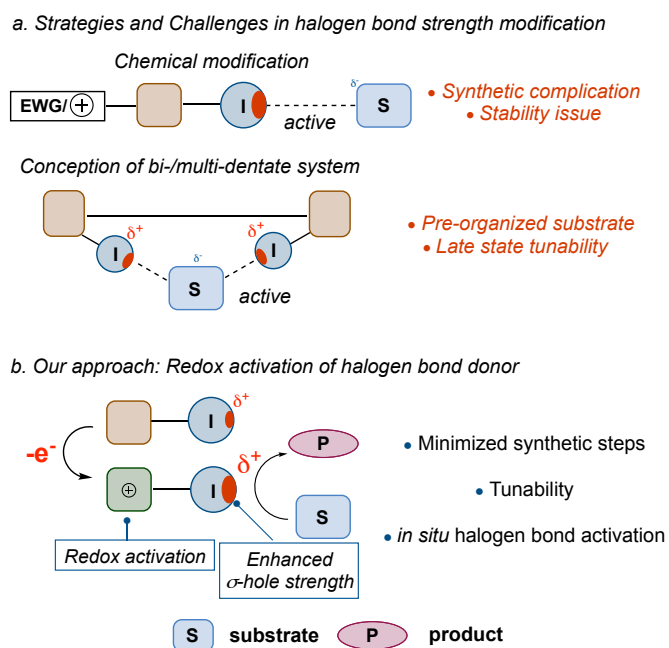


**Figure 1.** (a) Halogen bond strength modification strategies. (b) Redox activation of halogen bonding.

For decades, efforts to enhance the strength of the halogen bond donors, predominantly iodine-containing derivatives, have focused on two concept strategies.<sup>16–19</sup> The first involves chemical

<sup>a</sup> Sorbonne Université, CNRS, Institut Parisien de Chimie Moléculaire, IPCM, F-75005 Paris, France

<sup>b</sup> Université Paris Cité, CNRS, 75013 Paris, France

<sup>c</sup> Fakultät für Chemie und Biochemie, Ruhr-Universität Bochum Universitätsstraße 150, 44801 Bochum, Germany

<sup>d</sup> ITODYS UMR 7086, Université Paris Cité, CNRS, 75013 Paris, France

† Both authors contributed equally.

Supplementary Information available: [details of any supplementary information available should be included here]. See DOI: 10.1039/x0xx00000x



modification of the molecular scaffold by introducing electron-withdrawing groups (EWGs) and/or permanently charged moieties to electronically increase the strength of the XB (**Fig. 1a**). This approach provides great flexibility, enabling various molecular backbones in a manner that enhances the binding capacity of halogen bond donors. A second strategy consists of combining two or more XB donors to amplify and promote the halogen bond interaction. The main limitations arise from the strict geometric requirements inherent in the halogen bond, the intrinsic stability of the donor moieties, and solubility issues which complicate the rational design and synthesis of new XB donors.

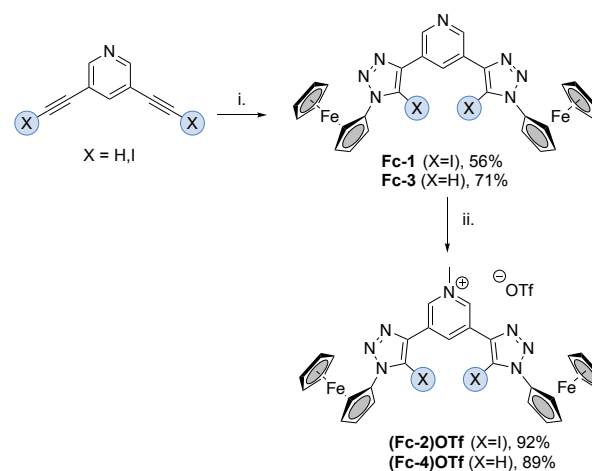
In recent years, redox activation has emerged as a powerful and innovative strategy for enhancing halogen bond donor strength (**Figure 1b**). In this approach, oxidation of the XB donor bearing redox-active moieties, such as tetrathiafulvalenes and ferrocene, increases the electrophilicity character of the halogen atom and thereby amplifying the value of its  $\sigma$ -hole.<sup>20–26</sup> This strategy opens new opportunities for deploying XB in organic synthesis. Several iodinated redox-active compounds, particularly those incorporating ferrocene units, have been reported and demonstrated to function as strong halogen bond donors in both anion sensing<sup>27–30</sup> and catalysis.<sup>31,32</sup> Despite these promising results, the broader use of redox activation to modulate halogen-bond strength remains relatively underexplored. The use of such reversible redox entities allows for a dynamic control of the halogen-bond interaction in solution. The ultimate goal of the present work is to trigger a catalytic reaction via the electrochemical switching of a tailored redox-active XB-donor catalyst as recently reported in C-N bond formation using anthracene derivatives.<sup>33,34</sup> Herein, we reported a novel molecular design strategy for iodoferrocene-derived XB donors. By leveraging the redox-active ferrocene core, we demonstrate a tunable ' $\sigma$ -hole' strength that facilitates halogen-bond-mediated Friedel–Crafts alkylation. Our findings highlight the role of charge induction by redox activation in stabilizing XB interactions within polar media, providing a versatile platform for redox-switchable catalysis.

## Result and Discussion

### Synthesis of the catalysts

**Fc-1** was designed as a bidentate redox active XB-donor catalyst based on a 3,5 disubstituted pyridine. The two ferrocenyl groups are directly linked to the iodotriazole moieties thus providing an efficient electronic communication with the halogen atoms *via* the  $\pi$ -conjugated system. However, the arrangement of these ferrocenyl-iodotriazol units in 3 and 5 position of the pyridine core prevents the direct electronic coupling between the redox active groups. The synthesis of **Fc-1** was accomplished in a single step *via* a modified Cu(I)-catalyzed azide–alkyne 1,3-dipolar cycloaddition between 3,5-diiodoethynylpyridine and azidoferrrocene in 56% yield (**Scheme 1**). The use of 3,5-diethynylpyridine instead, afforded the halogen free analogue **Fc-3** in 71% yield. Subsequent regioselective alkylation of **Fc-1** and **Fc-3** at the pyridine core with methyl

trifluoromethanesulfonate afforded the cationic species (**Fc-2**)OTf and (**Fc-4**)OTf in 92 and 89% yield respectively.



**Scheme 1.** Synthesis of ferrocene-based XB donors and non-XB donor analogues. Reaction conditions: (i) Cu(MeCN)<sub>4</sub>BF<sub>4</sub>, azidoferrrocene, tris-(benzyltriazolylmethyl)amine, diisopropylethylamine, CH<sub>2</sub>Cl<sub>2</sub>, 4 h, rt, 56 and 71% yield for **Fc-1** and **Fc-3**, respectively; (ii) MeOTf, CH<sub>2</sub>Cl<sub>2</sub>, 1 h, Ar, rt, 92 and 89% yield for (**Fc-2**)OTf and (**Fc-4**)OTf, respectively.

### Photophysical and electrochemical characterization of the catalysts in neutral state

To probe the electronic communication between the redox-active ferrocene scaffold and the halogen bond (XB) donor site, we performed UV-Vis spectroscopic studies in 1:1 dichloromethane/acetonitrile (**Table 1**). The fundamental *d-d* transition of the ferrocene core, observed at 427 nm, undergoes a subtle bathochromic shift to 437 nm in both **Fc-1** and **Fc-3**, upon conjugation with the triazole moiety. This shift is further intensified to 441 nm following *N*-methylation to the pyridinium core in (**Fc-4**)OTf, a result of the lowered LUMO energy induced by the potent electron-withdrawing nature of the quaternary heterocycle. In contrast, the presence of iodine in (**Fc-2**)OTf results in a weak hypsochromic shift to 436 nm. The  $\sigma$ -hole of the iodine donor effectively modulates the electron-deficiency of the pyridinium ring, thereby widening the HOMO–LUMO gap. However, the ability of the iodine donor to modulate the electronic environment of the ferrocene, even in the presence of a permanent positive charge, underscores the robustness of the charge-induction effect.



**Table 1.** Electrochemical and photophysical data for ferrocene derivatives and their respective oxidized species in 1:1 ACN/CH<sub>2</sub>Cl<sub>2</sub> solution. (Electrochemical cond : 0.25 mM Fc derivatives with 0.1 M *n*-Bu<sub>4</sub>NBF<sub>4</sub>. UV-vis cond: ~0.5 - 1.0x10<sup>-5</sup> M Fc-derivatives, optical path 1 cm.)

Compound	E <sup>1</sup> <sub>pc</sub> <sup>[a]</sup> (C-I)	E <sup>2</sup> <sub>pc</sub> <sup>[a]</sup> (py <sup>+</sup> )	E <sup>0</sup> <sup>[b]</sup> (Fc/Fc <sup>+</sup> )	λ <sub>max</sub> <sup>[c]</sup> (ε <sup>[d]</sup> ) (neutral state)	λ <sub>max</sub> <sup>[c]</sup> (ε <sup>[d]</sup> ) (ferricinium state)	t <sub>1/2</sub> <sup>[e]</sup> (oxidized state)
Fc	-	-	0.53	427 (170)	617 (641)	>24 h
Fc-1	-1.40	-	0.70	437 (718)	642 (1341)	15
(Fc-2)OTf	-1.64	-1.05	0.78	436 (1157)	642 (1421)	200
Fc-3	-	-	0.68	437 (635)	690 (851)	8
(Fc-4)OTf	-	-1.07	0.72	441 (900)	688 (984)	6

[a] reductive potential peak in V vs SCE; [b] Formal standard potential in V vs SCE; [c] wavelength maximum of absorption in nm; [d] molecular extinction coefficient in M·cm<sup>-1</sup>, [e] half-life time in min

Cyclic voltammetry (CV) of **Fc-1**, **(Fc-2)OTf**, **Fc-3**, and **(Fc-4)OTf** in a 1:1 mixture of dichloromethane/acetonitrile and 0.1 M tetrabutylammonium tetrafluoroborate (*n*-Bu)<sub>4</sub>BF<sub>4</sub> is shown in Figure 2 and Table 1. All ferrocene derivatives exhibit a reversible oxidation wave at the same formal standard potential of +0.73 ± 0.05 V vs SCE, which is about 200 mV more positive than ferrocene. This behaviour is similar to that reported by Molina and colleagues and is characteristic of the ferrocene attachment to the triazole rings at the N-1 position.<sup>29</sup> Surprisingly, the formation of the pyridinium ion results in a slight anodic shift in both cases (**Fc-1** relative to **Fc-2<sup>+</sup>** or **Fc-3** relative to **Fc-4<sup>+</sup>**), probably due to steric hindrance or reorganisation in solution. Similar diffusion coefficients have been determined for all investigated ferrocenes (D ~ 10<sup>-5</sup> cm<sup>2</sup>·s<sup>-1</sup>) suggesting their similar solubility and mobility in solution. The plot of the peak current versus the square root of the scan rate shows a linear trend accounting for a reversible diffusion limited electrochemical process meaning that the species freely diffuse in solution (Figures S7 to S10).<sup>35</sup>

In reduction, two different redox processes can be observed. **(Fc-4)OTf** and **(Fc-2)OTf** exhibit both an irreversible reduction peak centered at -1.07 V and -1.05 V vs SCE, respectively. This wave is attributed to the reduction of the pyridinium core and is only slightly affected by the chemical structures of the XB donors. A second irreversible wave appears for **Fc-1** and **(Fc-2)OTf** at -1.40 V and -1.64 V, respectively, corresponding to C-I bond cleavage. The significant difference of ~240 mV of the C-I bond cleavage wave suggests that this C-I bond is either bounded to the anion OTf or stabilized by electron-deficiency of the pyridinium ring, confirming the presence of halogen bonding in solution, and prompted us to further investigate the evidence in both solid and solution priors an investigation in catalysis.

## Evidence of halogen bonding in crystal and solution

**Evidence of halogen bonding in crystal structure.** X-ray diffraction of single crystals obtained for each compound are presented and discussed here (see ESI for more details and for the crystallization conditions). The resulting structural analyses provide further insight

into **Fc-1** and **Fc-3**. Both compounds crystallize in the monoclinic system, space group *P*<sub>2</sub><sub>1</sub>/*c*, albeit with different unit cell parameters. The centroids of the triazole rings were defined in order to determine the dihedral angles between the two triazoles and the attached iodine or hydrogen atoms (Table 2). Thus, the molecular arrangements of the two analogues differ significantly. In **Fc-1**, the two iodine atoms are oriented in opposite directions (dihedral angle ~124°, i.e., >90°), whereas in **Fc-3**, the triazole C-H groups are oriented in the same direction (dihedral angle ~54°, i.e., <90°). Weak intermolecular C-H...N and C-I...N interactions are observed for **Fc-3** and **Fc-1**, respectively, between the C-H or C-I group of one triazole and either the N atom of the pyridine ring or a N atom of a neighbouring triazole, thereby contributing to the overall packing arrangement.

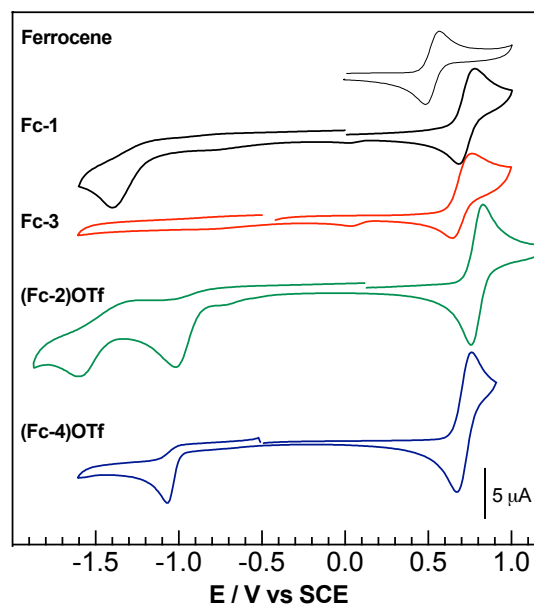


**Figure 2.** Cyclic voltammograms of 0.25 **Fc-1** (black), **Fc-3** (red), **(Fc-2)OTf** (green), **(Fc-4)OTf** (blue), and **ferrocene** (grey) versus saturated calomel electrode (SCE) as the reference and 0.1 M *n*-Bu<sub>4</sub>NBF<sub>4</sub> in 1:1 acetonitrile/dichloromethane as the electrolyte on a GC working electrode and Pt counter electrode; scan rate 0.1 V/s.



**Table 2.** Dihedral angle of (H1/I1-Triazole1-Triazole2-H2/I2) values in °.

Fc-1	Fc-3	(Fc-2)OTf	(Fc-2)I	(Fc-4)OTf
-124.537(18)	-53.706(2)	1.624(15)	3.639(11)	13.254(2) 32.804(2)

The methylated analogues (**Fc-2**)OTf and (**Fc-4**)OTf crystallize in the  $P2_1/c$  (monoclinic system) and the  $P-1$  (triclinic system) space groups, respectively. In the case of (**Fc-4**)OTf, two symmetry-independent molecules are present in the asymmetric unit. (**Fc-4**)OTf adopts a conformation similar to its neutral precursor **Fc-3**. In contrast, in (**Fc-2**)OTf, the two iodine atoms are oriented inward and engage in halogen bonding with the counter anion (**Figure 3**). The I...O distances (around 3.02 Å and 2.96 Å) are approximately 15% shorter than the theoretical sum of the van der Waals radii (3.50 Å). Moreover, the nearly linear C-I...O angles (~165.2–169.0°) clearly indicate highly directional halogen bonding.<sup>36,37</sup> This behaviour is not specific to triflate, as similar features are observed when iodide acts as the counter-ion in (**Fc-2**)I. In this structure, the I...I distances (around 3.34 Å and 3.46 Å) are approximately 18% shorter than the sum of the van der Waals radii (4.10 Å), and the more linear C-I...I angles (~172.3–173.2°) further highlight the presence of XB interaction in crystal state. Interestingly, in both iodinated structures, the dihedral angle between the two triazole rings is close to 0° (~1.6–3.6°), revealing an almost coplanar arrangement of the triazoles. For (**Fc-4**)OTf, weak intermolecular C-H...O interactions are observed between the triazole C-H groups and one oxygen atom of the triflate counter-anion. In addition,  $\pi\cdots\pi$  stacking interactions between certain Cp rings and the pyridine ring of a neighbouring molecule are also present. Similarly, in both (**Fc-2**)OTf and (**Fc-2**)I,  $\pi\cdots\pi$  stacking interactions between neighbouring triazole rings complement the XB interactions. In all three methylated derivatives, these non-covalent interactions act in concert to define the supramolecular architecture of the crystal.

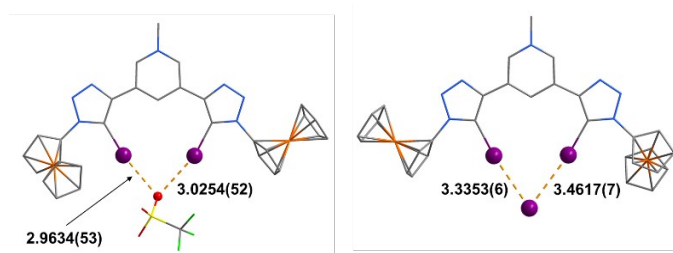


**Figure 3.** Crystal structure wireframe representations of (**Fc-2**)OTf (left) and (**Fc-2**)I (right). Atoms involved in halogen bonding are highlighted in ball drawing, the XB interactions are depicted as orange dashed lines and their distance values are indicated (Å). Atom colour code: purple (I), red (O), yellow (S), green (F), orange (Fe), blue (N), and grey (C). Hydrogen atoms, solvent molecules (ACN for (**Fc-2**)OTf and DMF for (**Fc-2**)I) as well as the second position of the disordered Cp group in (**Fc-2**)OTf, are omitted for clarity. Selected bond distances (Å) and angles (°). (Left) I...O: 2.9634(53)-3.0254(52), C-I...O: 169.071(235)-165.238(202), (Right) I...I: 3.3353(6)-3.4617(7), C-I...I: 173.179(142)-172.193(138).

**Evidence of halogen bonding in solution.** To evidence the formation of a XB complex in solution, various <sup>13</sup>C NMR spectra of **Fc-2**<sup>+</sup> in the presence of different anions have been recorded (**Figure S19** and

**S25**). The carbon C<sup>6</sup>, which is connecting to the iodine in pyridinium core received the strongest influence of anion. <sup>13</sup>C NMR in dimethylsulfoxide-d<sub>6</sub> exhibits a difference of ca. 35 ppm between iodide anion ( $\delta = 88.6$  ppm) and triflate anion ( $\delta = 124.4$  ppm). Interestingly, a significant downfield shift suggesting the heavy atom effect by iodide ion.<sup>38</sup> In addition to NMR, potentiometric titration was also performed to evaluate potential anion interaction through halogen bonding. Upon the addition of Cl<sup>-</sup> to **Fc-1** in 1:1 dichloromethane/acetonitrile mixture, the system exhibits a  $\Delta E$  of 21 mV with a small loss of reversibility suggesting a competition between halogen bonding interaction and chemical reaction (**Figure S11**). When a weak Lewis base is added in the solution almost negligible interaction has been recorded (**Figures S12** and **S13**), confirming these observations.<sup>21–23,27–29</sup> Thus our data obtained in both the crystal state and solution confirm the presence of halogen bonding. While the interaction is relatively weak, it prompted us to investigate further the oxidized forms of these complexes and their reactivity in chemical reactions.

### Ferrocenium **Fc-1**<sup>2+</sup>, **Fc-2**<sup>3+</sup>, **Fc-3**<sup>2+</sup> and **Fc-4**<sup>3+</sup>.

To assess the potential reactivity of the cationic complexes and achieve adequate stabilization of the ferrocenium species, we opted to investigate chemical oxidation. For this transformation – converting the neutral XB donors into their corresponding ferricenium cations **Fc**<sup>+</sup>**BF**<sub>4</sub><sup>-</sup> – we selected NOBF<sub>4</sub>, a well-known chemical oxidant.<sup>39</sup> First, to validate this oxidant toward **Fc** derivatives, we added 1.2 equivalents of NOBF<sub>4</sub> to a solution of **Fc** in 1:1 dichloromethane/acetonitrile mixture. This resulted in the emergence of a new absorption band at 617 nm, characteristic of a LMCT band of the **Fc**<sup>+</sup> cation (**Figure 4**).<sup>40,41</sup> UV-Vis absorption spectra of the oxidized dicationic states of the XB donors have thus been recorded following the same procedure. **Fc-1**<sup>2+</sup> displays a characteristic LMCT band at 642 nm (red trace in **Figure 4**) with an estimated half-life of 15 minutes (See ESI for more details). This band is slightly red-shifted in comparison to **Fc** ( $\Delta\lambda = 25$  nm), which could be attributed to the change in HOMO-1/LUMO gap in the presence of electron-withdrawing groups.<sup>42</sup> Meanwhile, oxidation of **Fc-3** by NOBF<sub>4</sub> afforded the corresponding ferrocenium **Fc-3**<sup>2+</sup>, with a further red-shifted absorption band at 690 nm. **Fc-3**<sup>2+</sup> appeared to be less stable ( $t_{1/2} \sim 8$  min, **Figures S3** and **S4**) than **Fc-1**<sup>2+</sup>. The increased persistent character of the iodinated species suggests a significant influenced by the presence of halogen atoms in **Fc-1**<sup>2+</sup>. In the tricationic species, the UV-vis spectra of **Fc-4**<sup>3+</sup> ( $\lambda = 688$  nm) and **Fc-2**<sup>3+</sup> ( $\lambda = 642$  nm) were similar to their respective non-methylated derivatives **Fc-3**<sup>2+</sup> and **Fc-1**<sup>2+</sup>. While the **Fc-4**<sup>3+</sup> displayed a similarly short lifetime ( $t_{1/2} \sim 6$  min) close to **Fc-3**<sup>2+</sup>, the iodinated analogue **Fc-2**<sup>3+</sup> showed remarkable stability with a measured half-life of about 200 minutes in solution (**Figure S5** and **S6**). This result highlights the synergetic effect between halogen bonding and molecular orientation in solution.



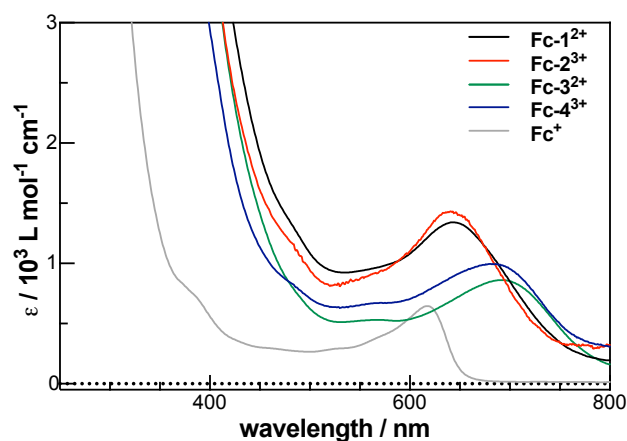


**Figure 4.** UV-Vis absorption spectra of **Fc-1<sup>2+</sup>** (black), **Fc-2<sup>3+</sup>** (red), **Fc-3<sup>2+</sup>** (green), **Fc-4<sup>3+</sup>** (blue), and **Fc<sup>+</sup>** (grey) in 1:1 dichloromethane/acetonitrile. Counter anions were omitted for clarity.

### Computational Details

Kohn–Sham density functional theory (DFT) as implemented in the Gaussian (G16) package was used for all computations,<sup>43</sup> employing the M06L<sup>44</sup> functional with D3 dispersion corrections.<sup>45</sup> The def2-TZVP basis set was used for all elements except I and F, which were treated with def2-TZVPD.<sup>46</sup> All structures were optimized in the gas phase and were confirmed as minima by the absence of imaginary frequencies. Calculations for **Fc-1** were conducted with charges 0 and +2, while charges +1 and +3 have been used for **Fc-2<sup>+</sup>**; in both cases the oxidized forms were more stable as triplets, as expected (Figure 5, see ESI for more details). For both pyridine and pyridinium compounds, the electrostatic surface potential (ESP) of the respective  $\sigma$ -holes exhibited the effect of permanent charge. The respective  $\sigma$ -holes potentials of **Fc-1** and **Fc-2<sup>+</sup>** increased from 34.6 to 86.2 kcal/mol, consistent with  $\sigma$ -hole amplification through chemical modification (Figure 5). Interestingly, oxidation of the two ferrocene units in **Fc-1** resulted in a 3.5-fold increase in  $\sigma$ -holes, which jumped to 120 kcal/mol, demonstrating the positive impact of the activation of halogen bond by redox activation. When redox activation was combined with a permanent pyridinium charge, the  $\sigma$ -holes value from ESP at iodine atoms in **Fc-2<sup>3+</sup>** increased further to 180 kcal/mol. Considering the  $\sigma$ -holes value of **Fc-1** the redox activation in the presence of permanently charged **Fc-2<sup>3+</sup>** could be increased up to fivefold in the  $\sigma$ -hole strength, indicating that redox chemistry provides an effective means to amplify the  $\sigma$ -hole on demand.

### Application in organic synthesis: redox activation of the XB donors for promoting Friedel-Crafts alkylation

DOI: 10.1039/D6SC02883G

The catalytic activity of the well-characterized bidentate XB donor catalysts, as well as their non-halogenated analogues, was then evaluated in organocatalytic reactions. The Friedel-Crafts alkylation reaction was selected as a benchmark due to its high sensitivity to Lewis acid activation, which allows for a clear quantification of the halogen bonding effect.<sup>47,48</sup> In fact, previous studies have established that bidentate XB donors can achieve significantly higher reaction rates compared to their hydrogen-bonding (HB) analogues in dichloromethane. The XB catalyst activates the labile C-X bond of benzhydryl halide thus accelerating the cleavage of the C-X bond and generating benzhydryl cation,<sup>49–52</sup> which promptly reacts with the nucleophilic 1,3,5-trimethoxybenzene **2** following a conventional electrophilic aromatic substitution mechanism.

**Friedel-Craft alkylation with C-Br bond cleavage.** The first Friedel-Crafts alkylations were performed using **Fc-1**. The active species, **Fc-1<sup>2+</sup>**, was generated by the addition of a **Fc-1** solution to NOBF<sub>4</sub> oxidant then transferred to a solution containing benzhydryl bromide **1** and 1,3,5-trimethoxybenzene **2** in an NMR tube. These primary screenings employed a stoichiometric amount of the XB donor and **1**, consistent with established literature protocols, and an excess of Cs<sub>2</sub>CO<sub>3</sub> to scavenge any Brønsted acids, thereby ruling out 'hidden' acid catalysis. To evaluate solvent effects on catalytic efficiency, screenings were conducted in dichloromethane-*d*<sub>2</sub> (CD<sub>2</sub>Cl<sub>2</sub>), 1:1 dichloromethane-*d*<sub>2</sub>/acetonitrile-*d*<sub>3</sub> (CD<sub>2</sub>Cl<sub>2</sub>/CD<sub>3</sub>CN), and acetonitrile-*d*<sub>3</sub> (CD<sub>3</sub>CN).

As shown in Table 3, in the presence of the activated catalyst **Fc-1<sup>2+</sup>** in CD<sub>2</sub>Cl<sub>2</sub>, product **3** was obtained in trace amount yield after 24 h, as expected for insoluble XB donor. Surprisingly, in a 1:1 mixture of CD<sub>2</sub>Cl<sub>2</sub>/CD<sub>3</sub>CN (entry 2, Table 3) the yield could be increased up to 59% (after 24 h). While this yield is moderate compared to the early reports in similar non-polar solvents (e.g., yields >90% in CH<sub>2</sub>Cl<sub>2</sub>),<sup>47</sup> our ferrocene-derived catalyst maintains catalytic activity in CH<sub>3</sub>CN, unlike previously reported bidentate XB donors, known to suffer from severe competitive inhibition in polar and coordinating solvents.<sup>48</sup>



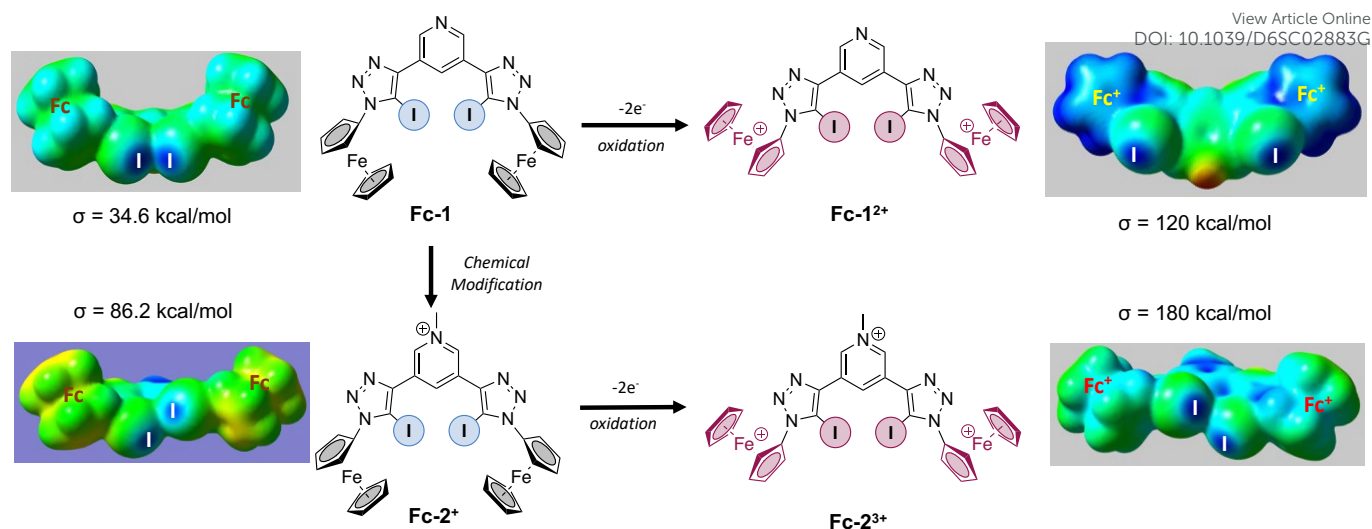
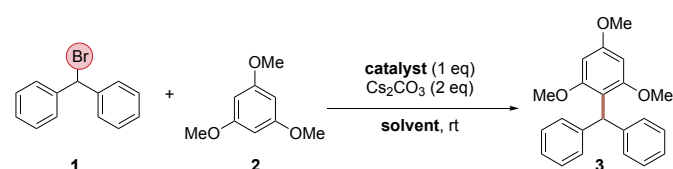


**Figure 5.** Molecular electrostatic potential surface mapped at the  $0.001 \text{ e.u.}^{-3}$  isovalue for the neutral and dication of **Fc-1** and monocation and trication of **Fc-2** with indication of its magnitude at the  $\sigma$ -hole (in kcal/mol). Note the different colour scale set from the extrema at the lowest and highest values in the molecule for each oxidation state.

**Table 3.** Reaction yields of product **3** in the Friedel-Crafts alkylation. <sup>[a]</sup>



Entry	Solvent	Catalyst	NMR yield <sup>[b]</sup>	
			2h	24h
1	CD <sub>2</sub> Cl <sub>2</sub>	<b>Fc-1<sup>2+</sup></b>	1	2
2	1:1 CD <sub>2</sub> Cl <sub>2</sub> /CD <sub>3</sub> CN	<b>Fc-1<sup>2+</sup></b>	54	59
3	CD <sub>3</sub> CN	<b>Fc-1<sup>2+</sup></b>	65	74
4	1:1 CD <sub>2</sub> Cl <sub>2</sub> /CD <sub>3</sub> CN	<b>Fc-2<sup>3+</sup></b>	80	98

[a] standard reactions conditions: 0.05 mmol of the catalyst in dry deuterated solvent under Ar, 1 eq. of **2**, 2 eq. Cs<sub>2</sub>CO<sub>3</sub>; [b] <sup>1</sup>H NMR Yields using *t*-amyl methyl ether as an internal standard.

In addition, in a pure acetonitrile solution, <sup>1</sup>H-NMR monitoring of the conversion yield revealed an acceleration of the reaction kinetics with a yield of 65% after only 2 h. After 24 hours, the yield was 74% (entry 3, **Table 3**), slightly higher in a CD<sub>2</sub>Cl<sub>2</sub>/CD<sub>3</sub>CN mixture. We attribute this observation to the unique redox-induced  $\sigma$ -hole strength amplification, which highlights the importance of the polar solvent in the reaction kinetics. However, due to the poor solubility in acetonitrile of the neutral XB donor in prior oxidation, the 1:1 CD<sub>2</sub>Cl<sub>2</sub>/CD<sub>3</sub>CN mixture seemed to us to be a good compromise and was used for further studies.

Based on the computational data, the presence of three positive charges in **Fc-2<sup>3+</sup>** should further enhance reactivity. In fact, the use of **Fc-2<sup>3+</sup>**, the oxidized form of **Fc-2<sup>+</sup>**, furnished the desired products in excellent yield (80% and 98%) within 2 h and 24 h, respectively (entry 4, **Table 3**). This suggested that the synergistic effect between the permanent positive charge and the redox activation enables such a

significantly strong XB donor. Indeed, by switching from **Fc-1<sup>2+</sup>** to **Fc-2<sup>3+</sup>**, we were able to increase the yield by approaching almost total conversion after 24 hours.

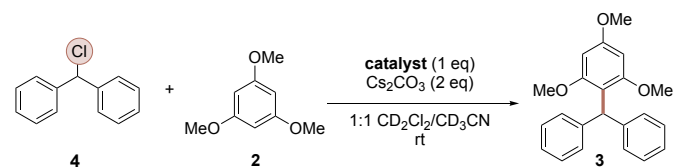
**Friedel-Crafts alkylation with C-Cl bond cleavage.** Encouraged by these results, we extended our study towards the benzhydryl chloride analogue **4**.<sup>53,54</sup> The main difficulty in using the chlorinated derivative **4** stem from the higher bond dissociation energy (BDE) of the C-Cl bond compared to the C-Br bond (74 vs 63 kcal/mol, respectively) making the C-Cl bond harder to cleave.<sup>55</sup> In a first attempt we tested the **Fc-1<sup>2+</sup>** in presence of **4**, in the same conditions as previously used with **1**. After 2 hours, the product **3** was obtained in 40% yield, suggesting a slightly slower kinetics profile than that of the brominated derivative **1** (**Table 4**, entry 1 vs. **Table 3** entry 2). However, in terms of thermodynamics, the **Fc-1<sup>2+</sup>** did not show any difference in efficiency. In fact, after 24 hours, a yield of 64% was obtained similar to that obtained with **1** (59%). As expected, the use of the tricationic **Fc-2<sup>3+</sup>** complex (**Table 4**, entry 2) induces a significant increase in reactivity compared to the **Fc-1<sup>2+</sup>** derivative, both kinetically (64% in 2 hours) and thermodynamically (70% in 24 hours) (**Table 4**, entry 2).

In order to confirm the fundamental impact of the halogen bonding in this Friedel-Crafts alkylation reaction, a series of control experiments was carried out. First, using non-oxidized or activated catalysts **Fc-1** and **Fc-2<sup>+</sup>** (**Table 4**, entries 3-4) completely hampered the reactivity with no detection of the expected product. This behavior can be attributed to the low value of  $\sigma$ -hole compared to their oxidized counterpart. Ferrocenium **Fc<sup>+</sup>** (**Table 4**, entry 5) and hydrogen bond donor **Fc-3<sup>2+</sup>** (**Table 4**, entry 6) also blocked the reactivity, suggesting that the reactivity did not originate from ferrocenium or other non-covalent interactions. Replacing the XB donor with elemental iodine (**Table 4**, entry 7) or with the *p*-toluenesulfonic acid (**Table 4**, entry 8) exhibited the formation of a



trace amount of product **3** (<5% yield) after 24 hours. All these findings strongly suggest that a strong halogen bonding is the key interaction promoting this reactivity. Moreover, the amplification of the  $\sigma$ -hole value is crucial for reactivity in polar solvents.

**Table 4.** Yield of product **3** in the reaction starting from **4**.<sup>[a]</sup>



Entry	Catalyst	Calculated $\sigma$ -hole <sup>[b]</sup>	NMR yield <sup>[c]</sup>	
			2h	24h
1	<b>Fc-1<sup>2+</sup></b>	120	40	64
2 <sup>[d]</sup>	<b>Fc-2<sup>3+</sup></b>	180	64	70
3	<b>Fc-1</b>	86.2	—	—
4	<b>Fc-2</b>	34.6	—	—
5	<b>Fc-3<sup>2+</sup></b>	—	—	—
6	<b>Fc<sup>+</sup></b>	—	—	—
7	<b>I<sub>2</sub></b>	—	—	<5
8	<b>p-TsOH</b>	—	—	<5

[a] standard reactions conditions: 0.05 mmol of the catalyst in dry deuterated solvent under Ar, 1 eq. of **2**, 2 eq. Cs<sub>2</sub>CO<sub>3</sub>; [b]  $\sigma$ -hole magnitude in kcal mol<sup>-1</sup>; [c] <sup>1</sup>H NMR yields using *t*-amyl methyl ether as an internal standard; [d] 4 times repetition with 1.25% as standard deviation.

Based on the combined experimental and DFT observations, we further hypothesized that, in the presence of a coordinating solvent, acetonitrile, the halide abstraction reaction might proceed catalytically. To test this hypothesis, we varied the loading of the **Fc-2<sup>3+</sup>** catalyst, the most active XB donor (**Figure 6**).

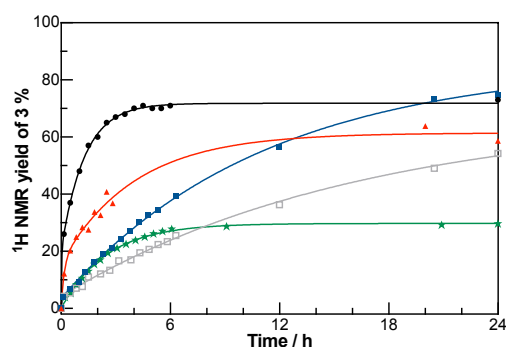


**Figure 6.** Yield vs. time diagram for the formation of **3** in the reaction from **4** in 100 mol% (8.33 mM, black circle), 50 mol% (4.17 mM, red triangle), 25 mol% (2.09 mM, blue square), 10 mol% (1.05 mM, grey empty square) and 2.5 mol% (0.26 mM, green star) of **Fc-2<sup>3+</sup>** catalyst. All reactions were conducted on a 0.05 mmol scale (8.33 mM), using dry 1:1 acetonitrile-*d*<sub>3</sub>/dichloromethane-*d*<sub>2</sub> solvent under Ar, 1 eq. of **2**, 2 eq. Cs<sub>2</sub>CO<sub>3</sub>. The yield of **3** has been determined according to <sup>1</sup>H-NMR analysis with *t*-amyl methyl ether as an internal standard.

While keeping the substrate concentration constants, reducing the catalyst loading to 50 mol% slightly diminished reactivity, yielding 60% of product **3** after 24 hours. This suggests that the reaction may indeed be catalytic. However, since the molecule contains two iodine

atoms, the observed reactivity could still be considered stoichiometric per iodine atom.

Further reducing the amount of the **Fc-2<sup>3+</sup>** to 25 mol% and 10 mol% had a noticeable impact on the initial reaction rate. Nevertheless, the system maintained remarkable reactivity under these conditions, delivering 75% and 52% yields for 25 mol% and 10 mol% of **Fc-2<sup>3+</sup>**, respectively. UV-vis analysis with substrates and 10 mol% **Fc-2<sup>3+</sup>** was also conducted, and the characteristic **Fc-2<sup>3+</sup>** absorption at 640 nm persisted for 18 h, indicating that the catalyst remains present in equilibrium with other species in solution (**Figure S15**). At the lowest catalyst **Fc-2<sup>3+</sup>** loading (2.5 mol%), reactivity dropped, with the yield failing to exceed 30% after 24 hours. This suggests that the catalyst is involved in the rate-determining step but remains catalytic, with a turnover number (TON) up to 10.

Additionally, since the plateau yield observed at 25 mol% catalyst loading after 24 hours is nearly identical to the yield under stoichiometric conditions, we further explored the role of catalyst concentration on the reaction kinetics. First, we examined how catalyst concentration affects the reaction, while maintaining constant the absolute ratio with compound **4**, *i.e.* 25 mol%. The reaction with a higher catalyst concentration (**Table 5**, entry 3) progressed significantly faster than the more diluted version (**Table 5**, entry 6). Although both conditions eventually reached a comparable maximum suggests that the reaction order with respect to total concentration is greater than zero, meaning that collisions between reactive species become a limiting factor under dilute conditions.

**Table 5.** Initial kinetics rate and NMR yield after 24 h of the standard (**Table 4**) with various catalyst and substrate loading.

Entry	Substrate loading <sup>[b]</sup>	Catalyst loading <sup>[c]</sup>	<i>k</i> <sub>rel</sub> <sup>[d]</sup>	NMR yield <sup>[e]</sup>
1	5	100	3.0	73
2	5	50	2.0	59
3	5	25	1	75
4	5	10	0.68	54
5	5	2.5	0.87	30
6	20	25	19	77

[a] standard reactions conditions: 0.05 mmol of the catalyst in 0.6 mL dry deuterated solvent under Ar, 2 eq. Cs<sub>2</sub>CO<sub>3</sub>; [b] substrate loading (both **2** and **4**) in  $\mu$ mol; [c] (**Fc-2<sup>3+</sup>**) loading (%); [d] Relative initial rates after 1 h of reaction time, referenced to entry 3; [e] <sup>1</sup>H NMR Yields using *t*-amyl methyl ether as an internal standard.

In a second step, we studied the impact of substrate concentration **4** while keeping the concentration of **Fc-2<sup>3+</sup>** constant. Interestingly, the substrate concentration had a less pronounced impact on the kinetic profile (**Table 5**, entry 1 and 6). By fixing the catalyst concentration, reactions conducted at  $\sim$ 8 mM or  $\sim$ 33 mM as concentration exhibited very similar kinetic profiles, both reaching a plateau of 70–75% yield within 6 hours. While the higher substrate concentration (33 mM) showed a faster initial rate, the difference was much less dramatic than the effect of varying the catalyst concentration. Even though this catalytic behavior is counterintuitive to typical halogen bonding reactivity, the catalytic activity may be



attributed to coordination by the polar solvent, which facilitates halide decoordination after abstraction and thereby regenerates the active XB donor.

## Conclusions

In conclusion, we have demonstrated the redox activation of chelating halogen bond donors for the promotion of a chemical reaction. A molecular bidentate system based on iodine-ferrocene architecture has been designed and its structure-property relationship investigated. We found that only ferrocenium XB donors **Fc-1<sup>2+</sup>** and **Fc-2<sup>3+</sup>** are chemically more stable than HB donors **Fc-3<sup>2+</sup>** and **Fc-4<sup>3+</sup>**, with a half-life of up to 4 h under Ar. Assessment of 'σ-hole' strength in the neutral and ferrocenium state revealed that redox activation is a powerful complement to structural modifications, enabling up to five times increase in 'σ-hole' strength relative to the neutral state of the redox couple. This redox-activation provided an opportunity to use oxidized XB donors in halide abstraction reaction affording TON = 10 at 2.5 mol% catalyst loading. We attribute this unprecedented catalytic performance to the presence of a coordinating solvent, which may act as a competing ligand, facilitating dynamic halide anion de-coordination in order to regenerate the XB-catalyst. While the consequences of these observations remain to be explored, their potential impact is of fundamental interest for exploring a broader scope of chemical transformations and designing new functional and more stable redox-active halogen bond donors for better control in organic synthesis.

## Author contributions

CF and BS conceptualized the project. CF, BS and SCK directed the project. SG, SA, UO, JF and SCK performed experiments. SMH performed calculation. All authors co-wrote the manuscript, discussed the results, and commented on the manuscript.

## Conflicts of interest

There are no conflicts to declare.

## Data availability

Supplementary information: Electrochemical investigation, NMR spectra and further experimental details. Crystal structures of **Fc-1**, (**Fc-2**)OTf, (**Fc-2**)I, **Fc-3** and (**Fc-4**)OTf were deposited at the Cambridge Crystallographic Data Centre with numbers CCDC 2536425 - 2536429 and can be obtained free of charge via [www.ccdc.cam.ac.uk](http://www.ccdc.cam.ac.uk).

## Acknowledgements

We acknowledge the Ministère de l'Enseignement Supérieur, de la Recherche et de l'Innovation, the Centre National de la Recherche Scientifique (CNRS). Elric Engelage and Geoffery Gontard for X-Ray

structures. SMH acknowledges Deutsche Forschungsgemeinschaft (DFG, German Research Foundation) under Germany's Excellence Strategy – EXC 2033 – 390677874 – RESOLV for access to a computational cluster.

## References

- D. W. C. MacMillan, *Nature*, 2008, **455**, 304–308.
- S. Bertelsen and K. A. Jørgensen, *Chem. Soc. Rev.*, 2009, **38**, 2178.
- C. Grondal, M. Jeanty and D. Enders, *Nature Chem*, 2010, **2**, 167–178.
- Z. Du and Z. Shao, *Chem. Soc. Rev.*, 2013, **42**, 1337–1378.
- V. Lyaskovskyy and B. De Bruin, *ACS Catal.*, 2012, **2**, 270–279.
- S. Martínez-Vivas, D. G. Gusev, M. Poyatos and E. Peris, *Angew Chem Int Ed*, 2023, **62**, e202313899.
- S. Acosta-Calle and A. J. M. Miller, *Acc. Chem. Res.*, 2023, **56**, 971–981.
- M. Erdelyi, *Nature Chem*, 2014, **6**, 762–764.
- L. C. Gilday, S. W. Robinson, T. A. Barendt, M. J. Langton, B. R. Mullaney and P. D. Beer, *Chem. Rev.*, 2015, **115**, 7118–7195.
- G. Cavallo, P. Metrangolo, R. Milani, T. Pilati, A. Priimagi, G. Resnati and G. Terraneo, *Chem. Rev.*, 2016, **116**, 2478–2601.
- P. J. Costa, *Physical Sciences Reviews*, DOI:10.1515/psr-2017-0136.
- S. Huber, Ed., *Halogen Bonding in Solution*, Wiley, 1st edn., 2021.
- P. Politzer, J. S. Murray and T. Clark, *Phys. Chem. Chem. Phys.*, 2013, **15**, 11178.
- G. R. Desiraju, P. S. Ho, L. Kloo, A. C. Legon, R. Marquardt, P. Metrangolo, P. Politzer, G. Resnati and K. Rissanen, *Pure and Applied Chemistry*, 2013, **85**, 1711–1713.
- P. R. Varadwaj, A. Varadwaj, H. M. Marques and K. Yamashita, *Crystal Growth & Design*, 2024, **24**, 5494–5525.
- D. Bulfield and S. M. Huber, *Chemistry A European J*, 2016, **22**, 14434–14450.
- R. L. Sutar and S. M. Huber, *ACS Catal.*, 2019, **9**, 9622–9639.
- M. Breugst and J. J. Koenig, *Eur J Org Chem*, 2020, **2020**, 5473–5487.
- D. Jovanovic, M. Poliyodath Mohanan and S. M. Huber, *Angew Chem Int Ed*, 2024, **63**, e202404823.
- S. Groni, T. Maby-Raud, C. Fave, M. Branca and B. Schöllhorn, *Chem. Commun.*, 2014, **50**, 14616–14619.
- R. Oliveira, S. Groni, C. Fave, M. Branca, F. Mavré, D. Lorcy, M. Fourmigué and B. Schöllhorn, *Physical Chemistry Chemical Physics*, 2016, **18**, 15867–15873.
- R. Oliveira, S. Groni, A. Vacher, F. Barrière, D. Lorcy, M. Fourmigué, E. Maisonhaute, B. Schöllhorn and C. Fave, *ChemistrySelect*, 2018, **3**, 8874–8880.
- H. Hijazi, A. Vacher, S. Groni, D. Lorcy, E. Levillain, C. Fave and B. Schöllhorn, *Chem. Commun.*, 2019, **55**, 1983–1986.
- C. Fave and B. Schöllhorn, *Current Opinion in Electrochemistry*, 2019, **15**, 89–96.
- M. S. Alvarez, C. Houzé, S. Groni, B. Schöllhorn and C. Fave, *Organic & Biomolecular Chemistry*, 2021, **19**, 7587–7593.
- E. Engelage, H. Hijazi, M. Gartmann, L.-M. Chamoreau, B. Schöllhorn, S. M. Huber and C. Fave, *Phys. Chem. Chem. Phys.*, 2021, **23**, 4344–4352.
- J. Y. C. Lim, M. J. Cunningham, J. J. Davis and P. D. Beer, *Chem. Commun.*, 2015, **51**, 14640–14643.



- 28 J. Y. C. Lim and P. D. Beer, *Eur J Inorg Chem*, 2017, **2017**, 220–224.
- 29 F. Zapata, A. Caballero and P. Molina, *European Journal of Inorganic Chemistry*, 2017, **2017**, 237–241.
- 30 N. Kim, V. S. Jeyaraj, J. Elbert, S. J. Seo, A. V. Mironenko and X. Su, *JACS Au*, 2024, **4**, 2523–2538.
- 31 V. Mamane, P. Peluso, E. Aubert, R. Weiss, E. Wenger, S. Cossu and P. Pale, *Organometallics*, 2020, **39**, 3936–3950.
- 32 E. Aubert, A. Doudouh, E. Wenger, B. Sechi, P. Peluso, P. Pale and V. Mamane, *Eur J Inorg Chem*, 2022, **2022**, e202100927.
- 33 A. HIRAMA, K. Suda, S. Yoshinaga, M. Kikuchi, S.-G. Chong, A. Kikuchi, Y. Ishigaki, D. Yokogawa, M. Atobe and N. Shida, *J. Am. Chem. Soc.*, 2026, jacs.5c18175.
- 34 A. HIRAMA, M. ATOBE and N. SHIDA, *Electrochemistry*, 2026, **94**, 037002–037002.
- 35 A. J. Bard, L. R. Faulkner and H. S. White, *Electrochemical methods: fundamentals and applications*, Wiley, Hoboken, NJ, USA Chichester, West Sussex, UK, Third edition., 2022.
- 36 A. Bondi, *J. Phys. Chem.*, 1964, **68**, 441–451.
- 37 I. Yu. Chernyshov, I. V. Ananyev and E. A. Pidko, *ChemPhysChem*, 2020, **21**, 370–376.
- 38 J. Vícha, J. Novotný, S. Komorovsky, M. Straka, M. Kaupp and R. Marek, *Chem. Rev.*, 2020, **120**, 7065–7103.
- 39 N. G. Connelly and W. E. Geiger, *Chem. Rev.*, 1996, **96**, 877–910.
- 40 H. B. Gray, Y. S. Sohn and N. Hendrickson, *J. Am. Chem. Soc.*, 1971, **93**, 3603–3612.
- 41 C. Swearingen, J. Wu, J. Stucki and A. Fitch, *Environ. Sci. Technol.*, 2004, **38**, 5598–5603.
- 42 F. S. T. Khan, S. Das and S. Hematian, *Journal of Coordination Chemistry*, 2025, **78**, 304–317.
- 43 M. ea Frisch, G. Trucks, H. B. Schlegel, G. Scuseria, Ma. Robb, J. Cheeseman, G. Scalmani, V. Barone, G. Petersson, H. Nakatsuji, and others, 2016.
- 44 Y. Zhao and D. G. Truhlar, *Theor Chem Account*, 2008, **120**, 215–241.
- 45 S. Grimme, J. Antony, S. Ehrlich and H. Krieg, *The Journal of Chemical Physics*, 2010, **132**, 154104.
- 46 F. Weigend and R. Ahlrichs, *Phys. Chem. Chem. Phys.*, 2005, **7**, 3297.
- 47 A. Dreger, E. Engelage, B. Mallick, P. D. Beer and S. M. Huber, *Chem. Commun.*, 2018, **54**, 4013–4016.
- 48 M. H. H. Voelkel, P. Wonner and S. M. Huber, *ChemistryOpen*, 2020, **9**, 214–224.
- 49 S. M. Walter, F. Kniep, E. Herdtweck and S. M. Huber, *Angew Chem Int Ed*, 2011, **50**, 7187–7191.
- 50 F. Kniep, L. Rout, S. M. Walter, H. K. V. Bensch, S. H. Jungbauer, E. Herdtweck and S. M. Huber, *Chem. Commun.*, 2012, **48**, 9299.
- 51 F. Kniep, S. M. Walter, E. Herdtweck and S. M. Huber, *Chemistry A European J*, 2012, **18**, 1306–1310.
- 52 F. Heinen, E. Engelage, A. Dreger, R. Weiss and S. M. Huber, *Angew Chem Int Ed*, 2018, **57**, 3830–3833.
- 53 A. Kerckhoffs, I. Moss and M. J. Langton, *Chem. Commun.*, 2023, **59**, 51–54.
- 54 Q. Jin, Y. Hai, L.-J. Liu, T.-G. Zhan and K.-D. Zhang, *Org. Chem. Front.*, 2025, **12**, 1217–1226.
- 55 S. J. Blanksby and G. B. Ellison, *Acc. Chem. Res.*, 2003, **36**, 255–263.

View Article Online  
DOI: 10.1039/D6SC02883G



# Redox Activation of Halogen-Bonding Catalysts for Organic Synthesis

View Article Online  
DOI: 10.1039/D6SC02883G

*Sihem Groni,<sup>a†</sup> Sercan Akbaba,<sup>b†</sup> Uchral Otgonbayar,<sup>a</sup> Jérémy Forté,<sup>a</sup> Stefan M. Huber,<sup>c</sup>  
Sitthichok Kasemthaveechok,<sup>\*a</sup> Bernd Schöllhorn<sup>\*d</sup> and Claire Fave<sup>\*a</sup>*

- Sorbonne Université, CNRS, Institut Parisien de Chimie Moléculaire, IPCM, F-75005 Paris, France
- Université Paris Cité, CNRS, 75013 Paris, France
- Fakultät für Chemie und Biochemie, Ruhr-Universität Bochum Universitätsstraße 150, 44801 Bochum, Germany
- ITODYS UMR 7086, Université Paris Cité, CNRS, 75013 Paris, France

## Corresponding Authors

\* email: [claire.fave@sorbonne-universite.fr](mailto:claire.fave@sorbonne-universite.fr); [sitthichok.kasemthaveechok@sorbonne-universite.fr](mailto:sitthichok.kasemthaveechok@sorbonne-universite.fr), [bernd.schollhorn@u-paris.fr](mailto:bernd.schollhorn@u-paris.fr)

## Data availability statement

Data are available upon reasonable request. Correspondence and requests should be addressed to [claire.fave@sorbonne-universite.fr](mailto:claire.fave@sorbonne-universite.fr); [sitthichok.kasemthaveechok@sorbonne-universite.fr](mailto:sitthichok.kasemthaveechok@sorbonne-universite.fr), [bernd.schollhorn@u-paris.fr](mailto:bernd.schollhorn@u-paris.fr)

